Optics Letters

Wavelength- and dispersion-tunable ultrafast holmium-doped fiber laser with dual-color operation

Maria Pawliszewska,[1,3] Anna Dużyńska,[2] Mariusz Zdrojek,[2] and Jarosław Sotor[1,4]

[1]Laser and Fiber Electronics Group, Faculty of Electronics, Wrocław University of Science and Technology, Wyb. Wyspiańskiego 27, 50-370 Wrocław, Poland
[2]Faculty of Physics, Warsaw University of Technology, Koszykowa 75, 00-662 Warsaw, Poland
[3]e-mail: maria.pawliszewska@pwr.edu.pl
[4]e-mail: jaroslaw.sotor@pwr.edu.pl

Received 20 November 2019; revised 10 January 2020; accepted 10 January 2020; posted 13 January 2020 (Doc. ID 383788); published 12 February 2020

We present a versatile ultrafast holmium-doped fiber laser with an intracavity Martinez compressor. The compressor enables continuous dispersion control, spectral filtering, and dual-color operation of the laser. Mode locking is supported for net cavity dispersion values ranging from highly anomalous (-1.42 ps^2) to net normal (0.3 ps^2), and wavelength tuning of the optical solitons is obtained in a 2021–2096 nm span. Dual-color pulsed operation of the laser is reached by implementing a mechanical bandstop filter within the compressor. The repetition rate offset of the two emitted frequency combs can be tuned in a 3–8 kHz range by adjusting the net cavity dispersion, or by changing the beam block diameter. We show that a relatively simple fiber resonator integrated with a Martinez compressor can serve as a highly tunable laser source.

https://doi.org/10.1364/OL.383788

The ongoing research on ultrafast fiber lasers operating in the > 2 μm spectral region is fueled by the variety of their applications, such as material processing, supercontinuum generation, or laser surgery [1]. Typically, new laser designs that provide higher average output power, decreased pulse durations, or improved stability are in demand. In certain applications, tunability of a laser is also a characteristic of interest. Wavelength-tunable pulsed light sources have found use in bioimaging [2] and spectroscopy [3]. Control over the emitted pulse duration is essential in micromachining, since it greatly affects the quality of the process [4]. Another important aspect to be considered while designing an ultrafast laser source is dispersion management. Choice of a dispersion operating regime affects the pulse formation mechanism, and therefore the performance of the oscillator [5]. In stretched-pulse lasers, where net cavity dispersion is close to zero, pulse durations below 100 fs can be reached [6], which is a significant improvement over solitonic lasers. In net-normal dispersion lasers, higher pulse energies can be obtained [7,8].

Dispersion control in a fiber laser can be performed by including fibers with opposing values of group delay dispersion (GDD) in the cavity [9–12]. Despite the advantages of an all-fiber setup, such an approach does not allow for continuous net cavity dispersion tuning due to the nature of the fiber splicing procedure. Furthermore, adding lengths of fiber to the resonator significantly affects the repetition frequency of the source. These issues can be addressed by utilizing a Martinez-style compressor [13]. To date, demonstrations of applying such compressors to thulium-, erbium- and ytterbium-doped fiber lasers have been presented [14–17]. By mechanically blocking parts of the spectrally dispersed beam, optical filtering can be obtained [14,18]. Another feature of such setups is the possibility to implement a mechanical bandstop spectral filter, which allows to reach dual-color operation of the laser, as presented in an ytterbium-doped fiber laser [19].

The majority of research on ultrafast holmium-doped fiber lasers concerns solitonic lasers based on both artificial [20] and real [21–23] saturable absorbers. In our recent reports, we have investigated dispersion-managed all-fiber holmium-doped lasers [12,24]; however, no setups utilizing more advanced means of dispersion compensation have been reported to date.

Here we present for the first time a widely tunable holmium-doped fiber laser with an integrated simplified Martinez compressor. The compressor based on a single transmission grating provides both wavelength and dispersion tuning capabilities. Mode-locked operation is supported from -1.42 to 0.3 ps^2 net cavity dispersion and in a 2021–2096 nm wavelength span. Additionally, dual-color operation is enabled by employing a mechanical bandstop filter. The proposed setup might serve as a versatile "performance on demand" radiation source for amplifier seeding, spectroscopy or basic science applications.

A schematic of the experimental setup is shown in Fig. 1. The oscillator is pumped by an in-house made thulium-doped fiber laser generating up to 3 W of output power. Pumping radiation is introduced to the cavity by a fused-type 1950/2080 nm wavelength-division multiplexer. A commercially available

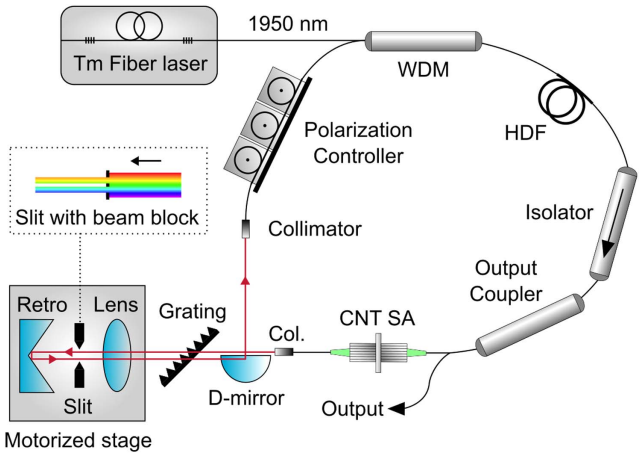

Fig. 1. Experimental setup. WDM, wavelength-division multiplexer; HDF, Ho-doped fiber; Retro, retroreflector; CNT SA, metallic carbon nanotube-based saturable absorber.

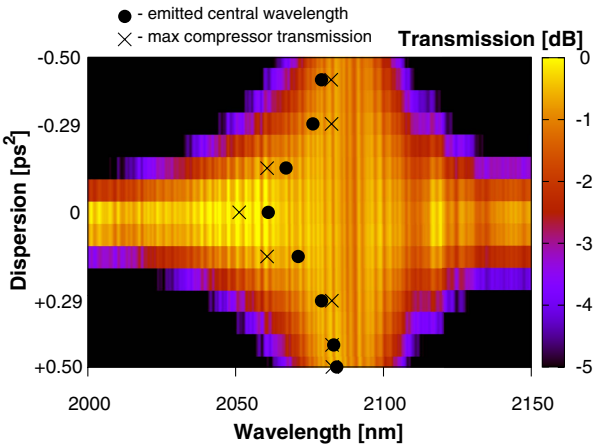

Fig. 2. Transmission of the Martinez compressor as a function of introduced dispersion. Circles: emitted central wavelengths [see Fig. 3(a)]; crosses: peak compressor transmission. Transmission values do not include insertion losses (65%).

holmium-doped fiber (iXblue IXF-HDF-8-125) serves as a gain medium. An isolator ensures unidirectional light propagation, while 30% of the signal is coupled out of the cavity. As a saturable absorber, a free-standing metallic carbon nanotube thin film inserted between two fiber connectors is used. Modulation depth of the 350 nm thick film used in the experiments is 5.5% (measured at 1950 nm). Thorough linear and nonlinear characterization of the nanomaterial is presented in Ref. [24].

The Martinez compressor based on a transmission grating (Ibsen Photonics FSTG-PCG-560-2000-930) with the absolute diffraction efficiency of 72% (for unpolarized light) is a non-fiberized part of the laser. Between the fiberized and bulk parts of the cavity, FiberPort (Thorlabs) collimators are used. A cylindrical lens ($f = 100$ mm) is placed together with a retroreflector on an electronically controlled motorized stage, forming a telescope. The simplified, folded architecture of the compressor is ensured by using a retroreflector—only one grating is therefore required as the beam crosses it twice. GDD introduced by the compressor is changed by modifying the distance between the telescope and grating. When said distance is equal to f, the compressor does not introduce any GDD. As calculated with the formula presented in Refs. [15,25], 1 mm of displacement from the neutral position of the compressor yields 0.015 ps^2 of GDD. The measured insertion losses of the compressor are at the level of 65% (including fiber coupling).

In order to determine the compressor's spectral transmittance as a function of introduced dispersion (shown in Fig. 2), a broadband light source was used. It is clearly seen that the effective bandwidth of the compressor decreases symmetrically with respect to the $4f$ position. It is a direct consequence of utilizing the simplified Martinez configuration with only two passes through the grating, which introduces spatial chirp and affects the bandwidth. The spatial chirp can be removed by additionally guiding the beam through a grating twice, or by designing a setup based on two gratings. However, such configurations are much more complicated and expensive and, most importantly, introduce additional insertion losses. The spectrum transmitted through the designed setup is also slightly affected by the interference fringes introduced by the bulk components, which, however, do not significantly affect mode-locked operation. An extra mechanical slit (Thorlabs VA100/M) inserted in the Fourier plane is employed to provide spectral filtering. Additionally, a beam block can be installed on the slit to implement bandstop filtering and support dual-color operation, which is discussed below. In all investigated resonator configurations, mode-locked operation is reached after increasing pumping power over a 700 mW level. A polarization controller can be used to slightly tune the central wavelength and bandwidth of the emitted pulses, although is not necessary for initializing pulsed operation.

The fiber part of the laser cavity consists of 1.94 m of the active fiber (GDD -0.102 ps^2/m) and 1.92 m of SMF-28 fiber (GDD -0.1 ps^2/m), which yields total GDD of -0.39 ps^2. The dispersion measurements were conducted with the use of a white light spectral interferometry technique [12,26]. While adjusting the dispersion introduced by the Martinez compressor, mode-locked operation was maintained from 0.3 ps^2 to -1.42 ps^2 net cavity GDD with the exception of a slightly net-normal region (between 0.01 and 0.06 ps^2), which can be attributed to limited modulation depth of the saturable absorber [27,28]. Beside this narrow unstable region, mode locking was constantly supported during dispersion tuning. Representative optical spectra registered for several GDD values are shown in Fig. 3(a).

For the net-negative dispersion values, distinctive Kelly sidebands can be observed. Both their spacing and bandwidth of the emitted pulses increase as the GDD approaches zero. The broadest, 20.6 nm wide spectrum was observed in the stretched-pulse dispersion regime at approximately 0 ps^2 of intracavity dispersion. The bandwidth corresponds to transform-limited pulse duration of 310 fs. As the GDD was increased, the spectra exhibited steeper, more rectangular shapes. All spectra were recorded at the pumping power of $\sim$ 750 mW, while the average output power was in the range of 12–14 mW.

The observed spectral shift of the emitted laser pulses [Fig. 3(a)] is directly connected to the transmission characteristics of the Martinez compressor (Fig. 2). When the compressor is set to the $4f$ position with the broadest transmission, the central wavelength of the emitted optical spectra (indicated with circles in Fig. 2) is determined by effective gain of the active fiber ($\sim$ 2060 nm [29]). However, when the dispersion of the compressor is tuned to normal or anomalous, the emitted spectra are shifted towards 2080 nm, which corresponds to the Martinez

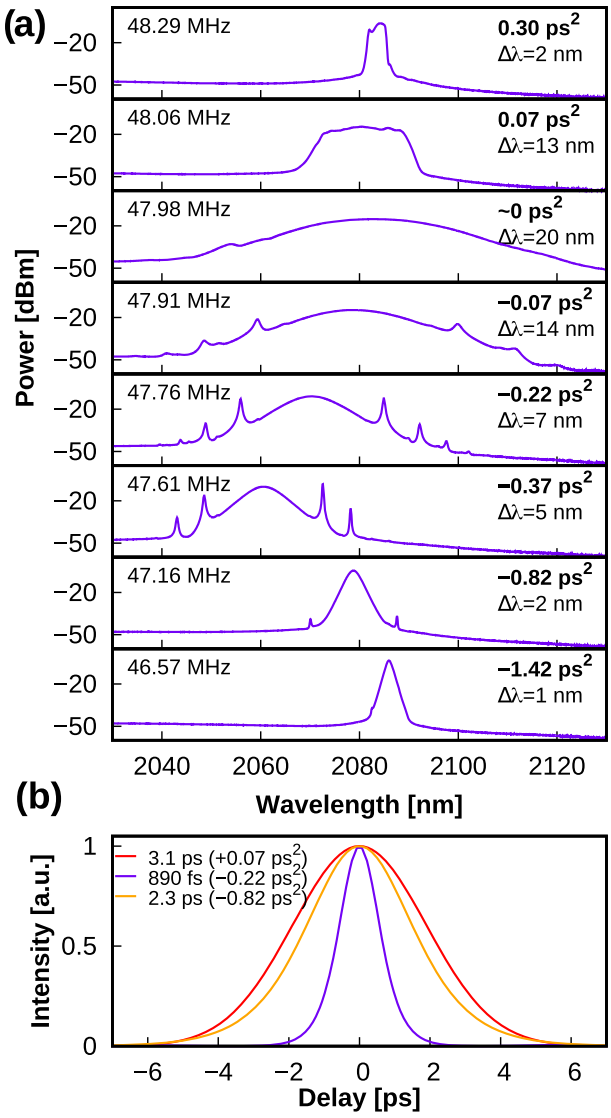

Fig. 3. (a) Spectrum evolution as a function of net cavity GDD. Repetition frequencies (left) and optical bandwidths (right) are indicated. (b) Autocorrelation traces of pulses emitted in anomalous and net-normal dispersion regimes measured directly at the laser output.

compressor's transmission maximum (indicated with crosses). The duration of the pulses generated in the net-normal dispersion regime exceeded 3 ps. Example autoccorelation acquired for GDD of 0.07 ps^2 is presented in Fig. 3(b). The generated solitons exhibited pulse durations ranging from 890 fs (GDD −0.22 ps^2) to nearly 4 ps for a very narrowband, 1 nm spectrum generated for net cavity dispersion of −1.42 ps^2.

Contrary to fiber-based dispersion compensation methods, utilizing a Martinez compressor allows to acquire large amounts of GDD while introducing minor changes to cavity length, and therefore the repetition frequency F_{rep}. In the experiment, the F_{rep} varied from 46.57 MHz (−1.42 ps^2) to 48.29 MHz (0.3 ps^2). Obtaining such a tuning range with the use of fibers with normal and anomalous GDD (starting from the resonator with net GDD of −0.39 ps^2 and F_{rep} of 47.6 MHz) would significantly reduce the F_{rep} to 17.42 MHz (adding 7.6 m of UHNA4 fiber) and 13.71 MHz (adding 10.6 m of SMF-28), respectively. The exemplary RF spectra registered for GDD of

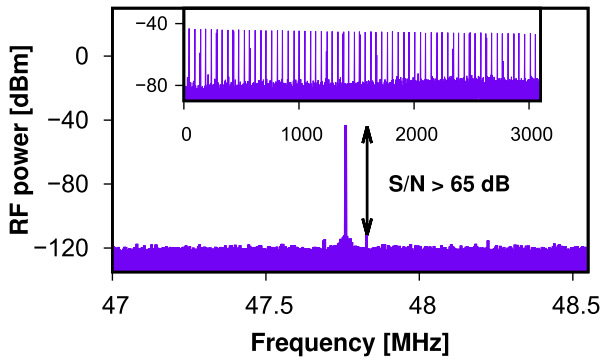

Fig. 4. Radio frequency spectra of the laser with net cavity GDD of −0.22 ps^2. Repetition frequency: 47.76 MHz, RBW: 50 Hz. RBW (inset): 470 kHz.

−0.22 ps^2 are shown in Fig. 4. The signal-to-noise ratio was on a satisfactory level of > 65 dB.

By adjusting the position of the slit relative to the spatially dispersed beam, continuous spectral tuning can be achieved. The widest tuning capabilities were observed while the spectral bandwidth of the filter was set to 10 nm. At fixed net cavity dispersion of −0.37 ps^2, mode-locking operation was supported while continuously tuning the central wavelength between 2021–2096 nm, which is shown in Fig. 5. The spectra undergo some spectral cropping, especially at the outermost edges of the supported wavelength range, which is caused by the limited gain bandwidth of the active fiber. Pumping power of ∼ 880 mW was used to maintain mode locking in the entire wavelength range.

To demonstrate versatility of the setup and provide dual-color operation of the laser, an additional beam block was used. For this purpose, pieces of optical fibers with varying diameters were placed on the slit to block the central part of the spectrum. The position of the beam block had to be manually adjusted in order to achieve dual-color mode locking instead of, e.g., single-pulse mode locking or continuous wave (CW) operation. For a beam block with 250 μm diameter, the repetition frequency difference (ΔF_{rep}) could be tuned in a 3.6–6.6 kHz range by altering the net cavity dispersion of the laser, as shown in Fig. 6(a). The influence of the beam block diameter on dual-color laser operation was also investigated. Optical fibers with 80, 125, 165, 250, 300, 450, and 690 μm diameters were used as beam blocks

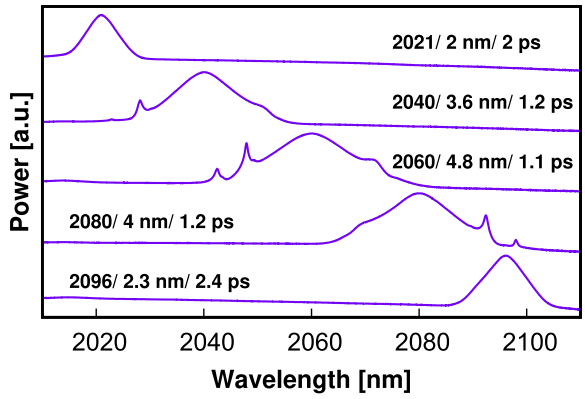

Fig. 5. Wavelength tuning capability of the laser. Central wavelengths, bandwidths, and temporal widths of the generated pulses are indicated for each trace.

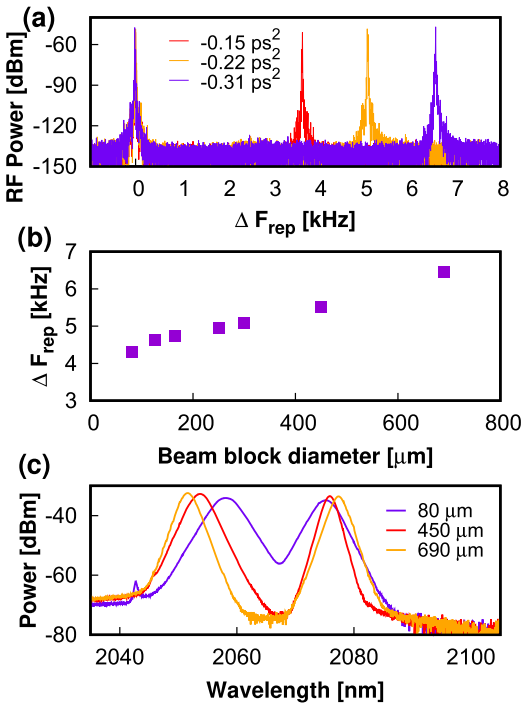

Fig. 6. (a) ΔF_{rep} for three net GDD values. The comb spacings are 3.66, 5.08, and 6.6 kHz. Beam block diameter: 250 μm, RBW: 1 Hz. (b) ΔF_{rep} dependence on beam block diameter at fixed net cavity dispersion of -0.22 ps^2. (c) Optical spectra of dual-color operation for three beam block diameters.

at fixed GDD of -0.22 ps^2 ($F_{rep} = 48.65$ MHz). As shown in Fig. 6(b), decreasing the spacing between two mode-locked spectra by using a narrower beam block reduces the separation between the generated solitons, which, due to chromatic dispersion, results in a smaller ΔF_{rep}. The influence of beam block diameter on the emitted optical spectrum is shown in Fig. 6(c). Standard deviation of ΔF_{rep} fluctuations measured over the course of 20 min is 12 Hz.

To determine the range of ΔF_{rep} supported by the setup, net GDD values for dual-color operation with the thinnest and thickest band blocks were experimentally established. For the 80 μm and 690 μm band block, the ΔF_{rep} range was 3.03–4.98 kHz and 4.78–8.05 kHz, respectively. In the context of potential application in spectroscopy, the smallest ΔF_{rep} value of 3.03 kHz supports the aliasing-free measurement range of 5.42 nm (0.39 THz) [30].

All presented measurements have been conducted with the use of the following measurement equipment: Yokogawa AQ6375 spectrum analyzer, Femtochrome FR-103XL autocorrelator, Keysight EXA N9010A RF spectrum analyzer (3.6 GHz), Discovery Semiconductors DSC2-50S photodiode (12 GHz), and Thorlabs PM100D power meter.

Summarizing, we have shown a highly tunable, passively mode-locked laser with dual-color operation capability. The intracavity Martinez compressor enables continuous dispersion tuning from highly anomalous (-1.42 ps^2) to net-normal (0.3 ps^2) dispersion regimes. Mode-locking operation is supported in a 2021–2096 nm wavelength span. Dual-color operation with adjustable comb spacing (3–8 kHz) is reached by utilizing a bandstop optical filter in the compressor. The presented source could serve as a relatively simple, yet highly flexible device with many practical applications.

Funding. Ministerstwo Nauki i Szkolnictwa Wyższego (IP2015 073774); Politechnika Wrocławska (0402/0110/18); Narodowe Centrum Nauki (2019/32/T/ST7/00223).

Acknowledgment. An author, Maria Pawliszewska, received financial support from Polish National Science Centre in a frame of doctoral scholarship (2019/32/T/ST7/00223).

Disclosures. The authors declare no conflicts of interest.

REFERENCES

1. J. Ma, Z. Qin, G. Xie, L. Qian, and D. Tang, Appl. Phys. Rev. **6**, 021317 (2019).
2. H. Chung, W. Liu, Q. Cao, R. Greinert, F. X. Kärtner, and G. Chang, IEEE J. Sel. Top. Quantum Electron. **25**, 1 (2019).
3. T. Hiraoka, T. Ohta, M. Ito, N. Nishizawa, and M. Hori, Jpn. J. Appl. Phys. **52**, 040201 (2013).
4. R. Le Harzic, D. Breitling, M. Weikert, S. Sommer, C. Föhl, S. Valette, C. Donnet, E. Audouard, and F. Dausinger, Appl. Surf. Sci. **249**, 322 (2005).
5. R. I. Woodward, J. Opt. **20**, 033002 (2018).
6. J. Sotor, I. Pasternak, A. Krajewska, W. Strupinski, and G. Sobon, Opt. Express **23**, 27503 (2015).
7. J. H. Im, S. Y. Choi, F. Rotermund, and D.-I. Yeom, Opt. Express **18**, 22141 (2010).
8. K. Kieu, W. H. Renninger, A. Chong, and F. W. Wise, Opt. Lett. **34**, 593 (2009).
9. Z. Zhang, Ç. Şenel, R. Hamid, and F. O. Ilday, Opt. Lett. **38**, 956 (2013).
10. K. Tamura, E. P. Ippen, H. A. Haus, and L. E. Nelson, Opt. Lett. **18**, 1080 (1993).
11. R. Kadel and B. R. Washburn, Appl. Opt. **54**, 746 (2015).
12. M. Pawliszewska, T. Martynkien, A. Przewłoka, and J. Sotor, Opt. Lett. **43**, 38 (2018).
13. O. Martinez, IEEE J. Quantum Electron. **23**, 59 (1987).
14. F. Haxsen, D. Wandt, U. Morgner, J. Neumann, and D. Kracht, Opt. Express **18**, 18981 (2010).
15. R. Lindberg, J. Bogusławski, I. Pasternak, A. Przewłoka, F. Laurell, V. Pasiskevicius, and J. Sotor, IEEE J. Sel. Top. Quantum Electron. **24**, 1 (2018).
16. K. Underwood and J. T. Gopinath, Opt. Lett. **41**, 5393 (2016).
17. L. Nugent-Glandorf, T. A. Johnson, Y. Kobayashi, and S. A. Diddams, Opt. Lett. **36**, 1578 (2011).
18. R. Dai, Y. Meng, Y. Li, J. Qin, S. Zhu, and F. Wang, Opt. Express **27**, 3518 (2019).
19. J. Fellinger, G. Winkler, A. S. Mayer, L. R. Steidle, and O. H. Heckl, Opt. Express **27**, 5478 (2019).
20. P. Li, A. Ruehl, C. Bransley, and I. Hartl, Laser Phys. Lett. **13**, 065104 (2016).
21. V. Dvoyrin, N. Tolstik, E. Sorokin, I. Sorokina, and A. Kurkov, *European Conference on Lasers and Electro-Optics* (OSA, 2015), paper CJ_7_4.
22. A. Y. Chamorovskiy, A. V. Marakulin, A. S. Kurkov, and O. G. Okhotnikov, Laser Phys. Lett. **9**, 602 (2012).
23. M. Hinkelmann, D. Wandt, U. Morgner, J. Neumann, and D. Kracht, Opt. Express **25**, 20522 (2017).
24. M. Pawliszewska, A. Dużyńska, M. Zdrojek, and J. Sotor, Opt. Express **27**, 11361 (2019).
25. E. Treacy, IEEE J. Quantum Electron. **5**, 454 (1969).
26. P. Hlubina, T. Martynkien, and W. Urbańczyk, Opt. Express **11**, 2793 (2003).
27. K. Kieu and F. W. Wise, in *Conference on Lasers and Electro-Optics* (OSA, 2009), paper CML3.
28. H. H. Liu and K. K. Chow, Opt. Lett. **39**, 150 (2014).
29. R. E. Tench, C. Romano, G. M. Williams, J.-M. Delavaux, T. Robin, B. Cadier, and A. Laurent, J. Light. Technol. **37**, 1434 (2019).
30. I. Coddington, N. Newbury, and W. Swann, Optica **3**, 414 (2016).